Remote Sensing in Ecology and Conservation
Open Access
ZSL LET'S WORK FOR WILDLIFE

ORIGINAL RESEARCH

Remote sensing liana infestation in an aseasonal tropical forest: addressing mismatch in spatial units of analyses

Chris J. Chandler[1], Geertje M. F. van der Heijden[1], Doreen S. Boyd[1], Mark E. J. Cutler[2], Hugo Costa[3,4], Reuben Nilus[5] & Giles M. Foody[1]

[1]School of Geography, University of Nottingham, University Park, Nottingham, United Kingdom
[2]School of Social Sciences, University of Dundee, Dundee, United Kingdom
[3]Direção-Geral do Território, Lisbon 1099-052, Portugal
[4]NOVA Information Management School (NOVA IMS), Universidade Nova de Lisboa, Campus de Campolide, Lisbon 1070-312, Portugal
[5]Forestry Department, Forest Research Center, Sandakan, Malaysia

Keywords
Hyperspectral imaging, liana infestation, LiDAR, neural network, pixel-based soft classification, segmentation

Correspondence
Chris J. Chandler, School of Geography, University of Nottingham, University Park, Nottingham, United Kingdom. Tel: +0115 951 5428; Fax: +0115 951 3666; E-mail: christopherjohnchandler@gmail.com

Editor: Mat Disney
Associate Editor: Karen Anderson

Received: 31 March 2020; Revised: 19 December 2020; Accepted: 14 January 2021

doi: 10.1002/rse2.197

Abstract

The ability to accurately assess liana (woody vine) infestation at the landscape level is essential to quantify their impact on carbon dynamics and help inform targeted forest management and conservation action. Remote sensing techniques provide potential solutions for assessing liana infestation at broader spatial scales. However, their use so far has been limited to seasonal forests, where there is a high spectral contrast between lianas and trees. Additionally, the ability to align the spatial units of remotely sensed data with canopy observations of liana infestation requires further attention. We combined airborne hyperspectral and LiDAR data with a neural network machine learning classification to assess the distribution of liana infestation at the landscape-level across an aseasonal primary forest in Sabah, Malaysia. We tested whether an object-based classification was more effective at predicting liana infestation when compared to a pixel-based classification. We found a stronger relationship between predicted and observed liana infestation when using a pixel-based approach (RMSD = 27.0% ± 0.80) in comparison to an object-based approach (RMSD = 32.6% ± 4.84). However, there was no significant difference in accuracy for object- versus pixel-based classifications when liana infestation was grouped into three classes; Low [0–30%], Medium [31–69%] and High [70–100%] (McNemar's $\chi^2 = 0.211$, $P = 0.65$). We demonstrate, for the first time, that remote sensing approaches are effective in accurately assessing liana infestation at a landscape scale in an aseasonal tropical forest. Our results indicate potential limitations in object-based approaches which require refinement in order to accurately segment imagery across contiguous closed-canopy forests. We conclude that the decision on whether to use a pixel- or object-based approach may depend on the structure of the forest and the ultimate application of the resulting output. Both approaches will provide a valuable tool to inform effective conservation and forest management.

Introduction

Lianas (woody vines) are a dominant plant functional type in tropical forests. Lianas use the structural composition of trees to reach the forest canopy, where they strongly compete with trees for light (Putz, 1984; Schnitzer, 2005). Recent studies have indicated that the presence of lianas may have a strong negative effect on tree diversity (Schnitzer & Carson, 2010), growth (van der Heijden & Phillips, 2009), recruitment (Stevens, 1987; Tymen et al., 2016), survival (Putz, 1984) and the ability of these forests to store and sequester carbon (Durán & Gianoli, 2013; van der Heijden et al., 2015). This is particularly relevant as tropical forests represent around 55% (471 ± 93 Pg C) of global carbon stocks (Pan et al., 2011) and thus are highly valued for their role in the

global carbon cycle. Therefore, liana proliferation, such as that observed in Neotropical forests (Phillips et al., 2002; Schnitzer & Bongers, 2011), may have global consequences for climate change.

Growing concern for the impact of lianas on the tropical forest carbon balance has led to an expansion of studies in recent years. However, the impact of lianas on tropical carbon budgets are usually studied from the ground (van der Heijden et al., 2015; Ingwell et al., 2010; Wright et al., 2015) with spatial extents limited to the order of plot size (typically, 0.1 ha to 50 ha) (Ingwell et al., 2010; Schnitzer et al., 2012). As the abundance and distribution of lianas may be influenced by processes that operate at multiple scales, field measurements that are constrained to small plots may restrict our understanding of the distribution and impact of lianas over larger areas. The ability to accurately assess liana infestation at a landscape level is therefore essential to quantify their impact on carbon dynamics and monitor change over time, which will assist in targeting conservation and management actions focussing on climate change mitigation in tropical forests.

Remote sensing may provide a solution to map liana infestation over larger areas than possible using field-based methods alone. Studies have shown clear differences in the spectral response of trees and lianas at the leaf- (Castro-Esau et al., 2004; Guzman et al., 2018; Hesketh & Sánchez-Azofeifa, 2012) and canopy levels (Kalacska et al., 2007; Sánchez-Azofeifa & Castro-Esau, 2006). Based on differences in the spectral response of trees and lianas, airborne-derived hyperspectral and LiDAR data have been used to effectively map liana canopy cover at a landscape level (Marvin et al., 2016). However, the use of remote sensing methodologies to map liana infestation at the landscape level have so far been limited to seasonal forests in the Neotropics (Foster et al., 2008; Li et al., 2018; Marvin et al., 2016). In aseasonal forests, a low spectral contrast between lianas and trees (Castro-Esau et al., 2004; Sánchez-Azofeifa et al., 2009) may pose an additional challenge for mapping liana infestation. Moreover in the study by Marvin et al. (2016) a disagreement between liana infestation predictions at the pixel-level (i.e., determined by the hyperspectral data) with field estimates at the object-level (i.e., per tree-crown) may have led to a reduction in classification accuracy. Such discrepancies in spatial units have been noted in multiple studies that have suggested the need to account for meaningful image objects in order to produce accurate land cover maps (Blaschke, 2010; Li & Shao, 2014; Yu et al., 2006).

The ability to spatially and temporally align ground observations of liana infestation with remotely sensed data is highly desirable to achieve an accurate classification. While aligning datasets in time is challenging due to the nature of data collection, the spatial units of remotely sensed data can be modified to accurately align with estimates of liana canopy cover. Liana infestation estimates at the pixel-level may be achieved by spectral unmixing of endmember pixels (Adam et al., 2016; Shao & Lan, 2019). Alternatively, LiDAR data may be used to delineate individual tree crowns (Jakubowski et al., 2013; Jing et al., 2014; Nunes et al., 2017), which can be used to segment hyperspectral imagery for an object-based classification. However, the effectiveness of an object-based approach may be compromised by errors caused by over- and under-segmentation (Chen et al., 2018; Liu & Xia, 2010).

Here, we examine, for the first time, whether a combination of airborne hyperspectral and LiDAR data can be used to accurately assess liana infestation across an aseasonal primary forest in Sabah, Borneo. By employing a neural network machine learning classification, we aim to predict liana infestation using both pixel- and object-based approaches and compare differences in their accuracies. We also discuss the potential benefits of pixel- versus object-based liana infestation outputs and their suitability for informing effective conservation and land management.

Materials and Methods

Study area

The study area is situated within the Danum Valley Conservation Area (DVCA), a primary lowland dipterocarp forest within the Yayasan Sabah (Sabah Foundation) forest concession (Reynolds et al., 2011) (Fig. 1). The DVCA (117°48'15.641"E, 4°57'54.822"N) remains a large and intact lowland forest (438 km^2). The climate is typical of the aseasonal tropics with an annual rainfall of around 2900 mm (O'Brien et al., 2019) and a mean annual temperature of 25.6°C (Fick & Hijmans, 2017).

Occupied airborne data collection

Occupied (or manned) airborne hyperspectral and LiDAR data were collected concurrently by the UK Natural Environmental Research Council's Airborne Research Facility (NERC-ARF) in November 2014. The data were captured from a Dornier 228–201, flying at 65.6–71.6 ms^{-1} at an altitude of 2335–2429 m. In total 10 flightlines were flown, on bearings of 100 or 280°, surveying an area of ~2083 ha of primary forest (Fig. 1).

LiDAR data were captured using a Leica ALS50-II which operates with an 8W class 4 laser with radiation at 1064 nm. The sensor is capable of recording up to four discrete returns for each emitted pulse. The footprint of the pulse on the ground is approximately 22 cm when

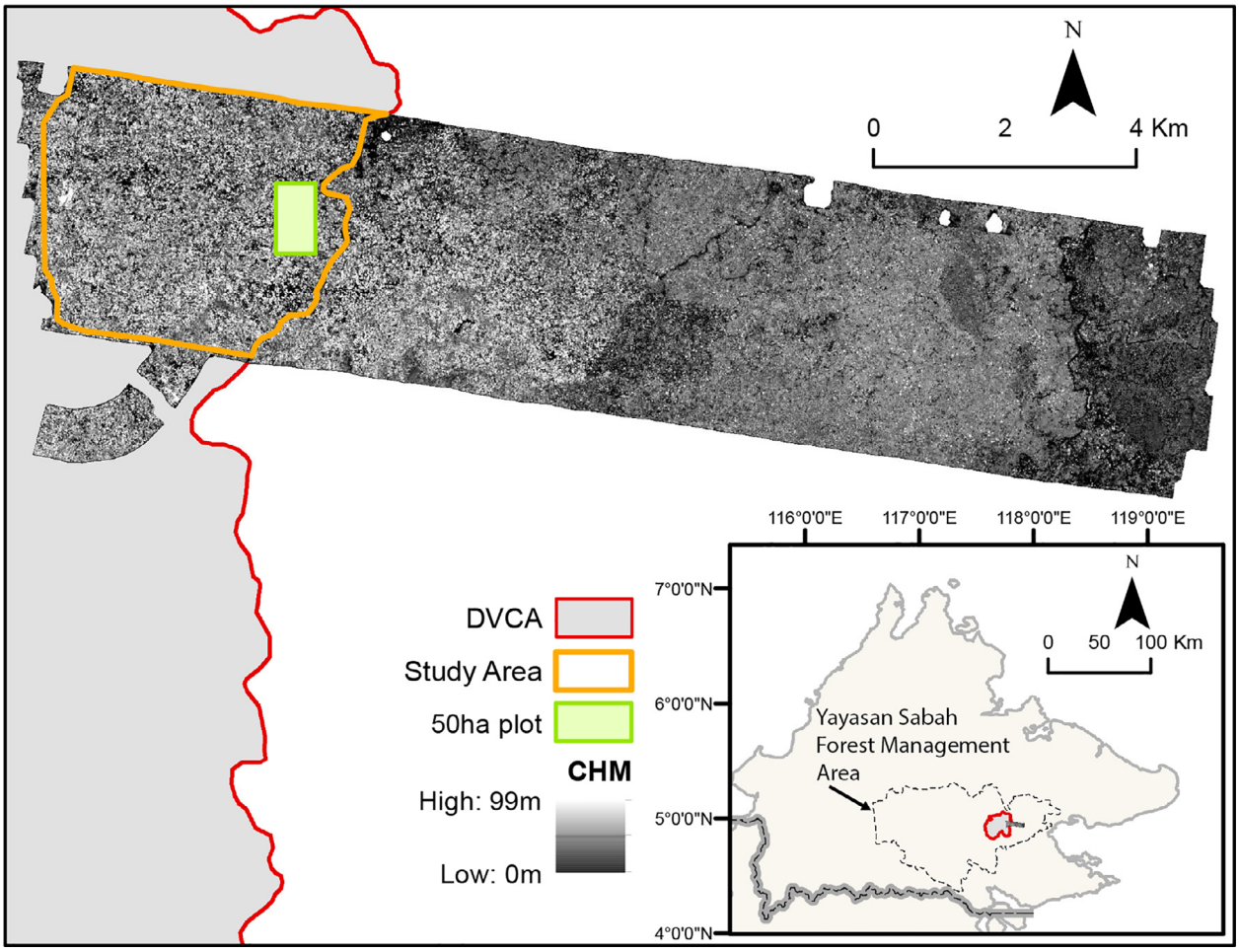

Figure 1. Location of the remotely sensed data and 50 ha plot in relation to the Danum Valley Conservation Area (DVCA) in Sabah, Malaysia. SFMA, Sabah Forest Management Area. The study area (orange line) as well as the 50-ha plot (green rectangle) are indicated. The Canopy Height Model (CHM) is used to represent the extent of the remotely sensed data.

fired from an altitude of 1000 m. The dataset has a point density ranging between 2.80 and 3.16 per m^2. The data were processed to produce a top-of-Canopy Height Model (CHM), with a spatial resolution of 1 m^2, based on the difference between the Digital Surface Model (DSM) and the Digital Elevation Model (DEM) using LAStools software (Isenburg, 2014).

Hyperspectral imagery were collected using a FENIX sensor (Specim Spectral Imaging, Finland), which acquired high resolution data from a large spectral range (380–2500 nm). Data were collected across 448 contiguous channels at a spatial resolution of 9 m^2. Spectral radiance sampled (2.9 nm) in the visible-to-near infrared (VNIR) ranged from 380 to 970 nm with a spectral resolution of 3.5 nm; in the shortwave infrared (SWIR) spectra were sampled (5.7 nm) from 970 to 2500 nm with a spectral resolution of 12 nm. Radiometric corrections were applied to the full hyperspectral dataset. Bands without data or those which were overly-saturated were removed. Data were atmospherically corrected using ENVI FLAASH (Fast Line-of-sight- Atmospheric Analysis of Spectral Hypercube) Atmospheric Correction (ENVI version 4.8, Exelis Visual Information Solutions, Boulder, Colorado). Post-correction quality checks revealed reflectance values varied between flightlines for the same individual pixels. As a result, all spectral values for individual flightlines were adjusted based on the difference in reflectance between overlapping pixels of adjacent flightlines (Taylor, 2001). An average of all pixels from one flight line were compared with an average of all overlapping pixels from the adjacent flightline. The average difference was calculated and adjusted for each band across the full flightline. All flightlines were combined and the dimensions of the data were reduced using a Standardised Principal Component Analysis (SPCA) to account for differences in spectral reflectance between flightlines.

SPCA uses a correlation matrix which has the same effect as using normalised bands of unit variance (Chang & Yoon, 2003). The first 8 principal components (raster layers) were retained, which explained more than 99% of the variation. Lastly, the 8 principal component values were scaled using a min-max normalisation:

$$\frac{p_{\mathrm{pc}} - \min\left(p_{\mathrm{pc}}\right)}{\max\left(p_{\mathrm{pc}}\right) - \min\left(p_{\mathrm{pc}}\right)} \quad (1)$$

where p_{pc} is the value for each pixel within each of the eight principal component layers.

Liana canopy cover survey

Data on liana canopy cover were collected in 2017 and 2018 for training of a neural network classification ($n = 454$ trees). The LiDAR data were uploaded to a tablet computer (Apple) connected to a GPS receiver (Garmin GLO 2; GARMIN) so individual tree crowns could be visually delineated in the field using the GeoEditor application (MapTiler). As a result, error associated with GPS accuracies can be avoided. To minimise error associated with estimating liana canopy cover, effort was taken to ensure each tree crown was thoroughly and accurately assessed by; (1) only recording tree crowns that were identified on the canopy height model with a high degree of certainty, (2) making sure tree crowns were fully sun-lit and completely unobscured from above and (3) having a minimum of two people independently estimating the percentage of a tree crown infested with lianas to the nearest 5% and then mutually agreeing on a final estimate (*cf.* Marvin et al., 2016).

Tree crown segmentation

The CHM was segmented using the *meanshift* algorithm in the Orfeo Toolbox (OTB) within QGIS v3.6.0 (QGIS Development Team, 2018). The segmentation output consisted of a set of contiguous and non-overlapping objects. The *meanshift* algorithm was controlled by three main parameters: scale, radius and threshold. We performed a grid-search using four different values for each parameter (Table S1). A total of 64 segmentations were produced using each parameter combination (Table S2). It is not possible to know, prior to segmentation, which combination of values will produce the optimal segmentation, therefore a large range of values were chosen for each parameter to ensure the optimal parameter combination was captured. Following this, a second grid search was performed which inspected an additional 27 combinations (Table S3). Each segmentation result was submitted to a supervised accuracy assessment. Among the many methods available (Costa et al., 2018), the Segmentation Evaluation Index (SEI) (Yang et al., 2015) was selected to provide an estimate of the accuracy of the segmentation. SEI is a strict measure as it requires a one-to-one correspondence between the segments and reference polygons. This is a desirable feature in the context of this study as one object should correspond to just one tree and vice versa. If not, the segmentation accuracy is penalised (Costa et al., 2018). The 91 segmentations were compared against a reference set of 124 tree boundaries across the study area manually delineated using the CHM. SEI values ranged from 0.276 to 0.818, corresponding to the best and worse results, respectively. The smallest SEI value was derived from the parameter combination: scale = 15, radius = 5 and threshold = 0.005 (Table S3). The segmentation produced with this parameter combination was used in the subsequent analysis.

Hyperspectral data extraction

When assessing liana canopy cover from the ground, it is only possible to estimate liana infestation for entire tree-crowns (objects). A more detailed assessment of liana infestation within a tree crown can be achieved by visually dividing the crown into quadrants (*cf.* Marvin et al., 2016). In either case, estimates of liana infestation when assessed from the ground cannot be achieved at the same scale of the hyperspectral pixels. To overcome this, we derived end-member spectra from trees without lianas in their canopy (therefore 'tree') and trees with highly liana infested (≥75%) canopies (therefore 'liana') to explain the spectral range (Plaza et al., 2012). As such, each hyperspectral pixel within the object relates to a pure cover of either tree or liana leaves. To allow comparison with the object-based approach, we derived end-member spectra for both approaches (Fig. 2). For the object-based classification, end-member spectra were extracted from the segmented hyperspectral imagery for the same trees used in the pixel-based classification ($n = 267$ trees/8827 pixels; Table 1). This yielded a total of 7826 hyperspectral pixels (226 trees) with no liana infestation and 1001 hyperspectral pixels (41 trees) with highly liana-infested canopies (see, Table 1).

Where the crown delineation derived from the CHM overlapped more than one object in the segmented hyperspectral imagery, we assigned a weight based on the proportion of each segmented object that made up the area as defined by the delineated crown boundaries. All weights were normalised to add up to one and used to calculate a weighted mean by multiplying the spectral values of a segmented object with the associated weight.

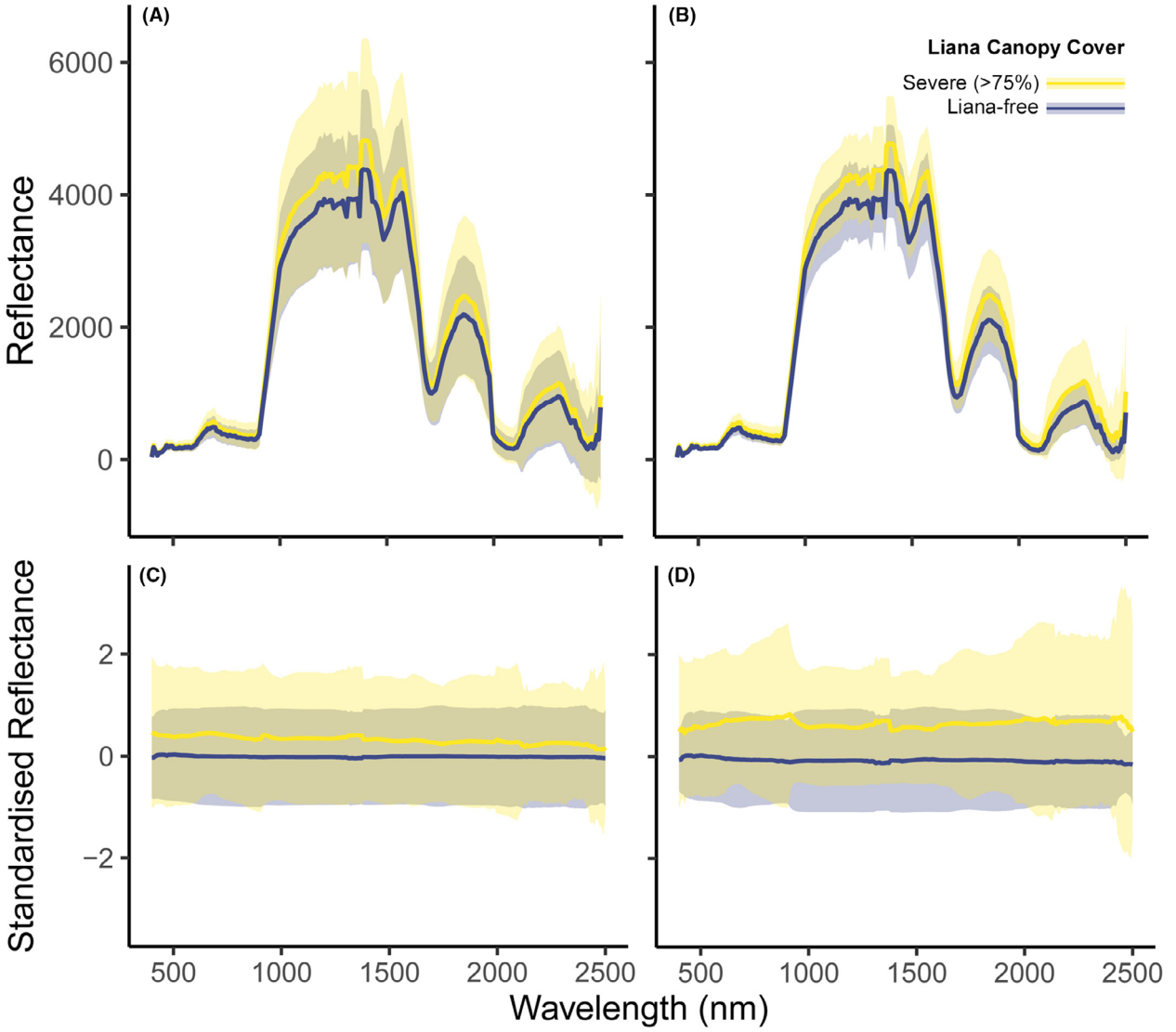

Figure 2. Spectral reflectance of liana-free trees and trees highly infested with liana leaves using ground-based training data. (A and B) Average reflectance values for pixel- and object-based approaches, respectively. (C and D) Standardised reflectance values for pixel- and object-based approaches, respectively. Standardised ($\mu = 0$, $\sigma = 1$) reflectance shows the difference across all bands by removing the magnitude of reflectance. Lines are mean reflectance values for all trees (shading $\pm$ 1 SD). Blue lines represent liana-free trees ($n_{trees} = 226$, $n_{pixels} = 7826$), yellow lines represent trees highly infested with liana leaves ($n_{trees} = 41$, $n_{pixels} = 1001$).

Table 1. Data used for the training of neural network models and validation of predicted liana infestation maps.

Approach	Spatial unit	Training data	Total EMs	EMs [0%]	EMs [>75%]	Balanced EMs [0, 75%]	EMs (80%) training [0, >75%]	EMs (20%) testing [0, >75%]	Valid. data (#trees)
Pixel Output P	9 m^2 Pixel	**14 552**	**8827**	7826	1001	**2002**	1602	200	168
Object Output O 168	Tree	crown	**454**	**267**	226	41	**82**	66	16

EMs, Endmembers; values within [ ] indicate proportional coverage of liana infestation in the tree crown. Balanced EMs contain an equal number of data points within each class. Numbers in bold refer to totals.

Neural network modelling

To predict liana infestation across the landscape we used a neural network model. Machine learning classifications such as neural networks often perform well when dealing with large datasets that include variables with non-linear, complex relationships. Unlike many other prediction techniques, they can learn hidden relationships without imposing restrictions such as fixed relationships in the data. We used a neural network model with resilient backpropagation and weight backtracking, which is often faster than regular backpropagation as parameters such as learning rate and momentum are not required to achieve optimal convergence time (Yu & Liu, 2002). The model architecture consisted of an input layer with eight principal components and canopy height, one hidden layer with 6 units (neurons) and an outputs layer with two units which correspond to either a tree or liana class. Tree height was used as an input variable as it has shown to be a key driver in the spatial distribution of lianas (Dalling et al., 2012; Meyer et al., 2019). The number of hidden units were defined subjectively based on trial runs (see Table S4.). The optimal model consisted of one hidden layer with 4 neurons, thus the architecture took the form of 9 : 4 : 2 for input : hidden : output units, respectively. A sigmoid activation function was applied to the hidden units and therefore the outputs values were restricted to a range between 0 and 1, that is, $\sigma(x) \in (0, 1)$. The output from the neural network represents a measure of the strength of class membership, and so may be used to generate a soft classification output, in this case, the proportion of liana infestation cover (Foody, 1997; Foody, 2000).

Prior to training the neural network model, the liana-free and severely liana-infested data were balanced by randomly removing pixels without liana infestation to ensure there was an equal number of data points within each input class (i.e., 1001 pixels for each class). The pixels for each class were then randomly split into 80% for training (801 pixels) and 20% for verification (200 pixels) (Olson et al., 2018).

We recognise that liana canopy cover estimates may have changed during the time lag (2.5–3.5 years) between airborne data acquisition and liana canopy cover surveys. Subsequently, both an increase and decrease in liana infestation may have occurred during this time. For example, the formation of a new canopy gap would be prone to rapid liana colonisation. While knowledge on the temporal dynamics of liana infestation is scarce, two studies—one in a seasonal (Ingwell et al., 2010) and one in an aseasonal forest (Wright et al., 2015)—give some insights into the size of the change in liana infestation that can be expected. A study conducted in an aseasonal forest in peninsular Malaysia revealed that 2% of trees that had no liana infestation had become severely (≥75%) liana infested, and vice versa, over a 12-year period (Wright et al., 2015). The change in the seasonal forest was greater, with Ingwell et al. (2010) observing that 5.3% of trees had changed from no liana infestation to severely (≥75%) liana infested; and 10.9% of trees had changed from severely liana infested to no liana infestation over a 10-year period. The difference between the two studies can be explained by the rapid growth, and the growth advantage, of lianas over trees in seasonal forests (Schnitzer et al., 2019). Although these data show that it is unlikely that substantial changes in liana infestation would have occurred over a 3.5-year time frame, we nevertheless accounted for a potential large difference in liana canopy cover estimates by applying noise to the input data that represented the same degree of change observed by Ingwell et al. (2010). To incorporate a similar size error as in Ingwell et al. (2010), we randomly selected 42 pixels or 2 trees (5.3% of the input data, pixels or objects respectively) from the class with no liana infestation and classified them as severely liana infested. Similarly, we randomly selected 87 pixels or 4 trees (10.9% of the input data, pixels or objects, respectively) from the class with severe liana infestation and classified them as liana-free.

The neural network model was run 100 times and after each iteration the model was applied to the entire study landscape. With each iteration we randomly (1) removed pixels from the no liana infestation class to ensure each input class was balanced, (2) split data for training and verification and (3) reclassified a proportion of the input data to account for differences in liana canopy cover estimates over time (as above). The final landscape scale liana infestation output is an average of all 100 neural network iterations. Averaging multiple models improves generalisation and also allows the calculation of uncertainty estimates based on the standard deviation of all predictions (Lu et al., 2008). To assess the level of uncertainty across predictions, we regressed the standard deviation for predicted values, from 100 runs of the neural network, against liana infestation.

Separately to this, we also assessed the maximum degree of error which could be applied to the input data without a significant loss in the accuracy of predicted liana infestation. We incrementally increased error in the input data from 0% to 50% over 100 neural network model iterations to assess the effect of input data inaccuracies on the neural network model error and classification accuracy. An incremental increase of noise in the input data with each iteration of the neural network revealed a steady increase in the neural network sum of squared error (Fig. S4). However, the ability of the neural network to generalise is maintained up to 30% error in the input data as shown by the accuracy of model predictions in relation to a verification dataset. The use of input data with 16% error, as observed by Ingwell et al. (2010), shows to have little impact on the accuracy of predicted liana infestation.

Accuracy assessment of predicted outputs

Following good practice for accuracy assessment (Olofsson et al., 2014; Stehman & Foody, 2019), we used an independent dataset of trees ($n = 168$) collected in a random distribution from within the 50 ha plot to assess the accuracy of the predicted map (Fig. 1; Table 1). We used a weighted mean approach (see Section 2.5) to account for cases where tree crown boundaries of segmented objects did not match perfectly with crown boundaries delineated using the CHM in the field. To validate the pixel-based classification, we averaged predicted liana infestation values for individual pixels inside the delineated crown boundaries to derive liana canopy cover estimates at the tree level.

To assess the accuracy of predicted liana infestation maps, we estimated the root mean squared deviation (RMSD) as follows:

$$\mathrm{RMSD} = \sqrt{\frac{1}{n-1}\sum_{i=1}^{n}(\hat{y}_i - y_i)^2} \quad (2)$$

which represents the mean deviation of predicted from observed values (i.e., with respect to the 1:1 line) (Piñeiro et al., 2008). Assessing the accuracy of model predictions imposes special interest in the 1:1 line of equality, $Y = X$. Unlike the root mean squared error (RMSE) which estimates the mean deviation of predicted values from the regression line of predicted vs observed values, the RMSD calculates the deviation of each predicted value against the 1:1 line (Gauch et al., 2003). Subsequently, RMSE will always be smaller and thus an underestimation of the error between observed and predicted values (Piñeiro et al., 2008). The units of RMSD correspond to the same units as the model variable under evaluation, in this case the percentage of liana infestation.

We accounted for error associated with observational uncertainty in liana canopy cover estimates as well as temporal change applied in model training. We quantified observational error by assessing the difference between estimates of liana canopy cover derived from two observers. The mean difference in estimates were used to obtain a small and gross observational uncertainty (Fig. S5). Data revealed that 96% of trees contained a small error of 5% and 4% of trees contained a large error of 30% (Fig. S5). Error derived from temporal change was also applied whereby 8% of trees had an error of 75% (see Data S1, section 1.6). Observed liana canopy cover values were entered into Monte Carlo (MC) simulations. Random values were generated from a t-distribution with a variation that encompassed the three levels of error (i.e., 5%, 30% and 75%). Using this approach we generated 100 random values which could be used to assess each of the 100 predicted liana infestation maps.

We also degraded outputs to an ordinal scale by partitioning predicted liana infestation into three groups as follows: neural network membership values equal to or below 0.3 were set to 'low', values between 0.31 and 0.69 were set to 'medium' and values equal to or greater than 0.7 were set to 'high'. We produced a confusion matrix using predicted and reference liana infestation grouped in three classes. We used overall accuracy and Area Under the Curve (AUC) to assess the accuracy of predicted values. To test for significant differences between pixel- and object-based approaches we used a McNemar test to assess the level of consistency between the two model outputs. A 0.05 significance level was used. All analyses were conducted in R v3.5.1 (R Core Team, 2019).

Results

Spectral difference between liana-free and highly liana infested trees

We found spectral differences between liana-free trees and trees highly infested with lianas for both pixel- (Fig. 2A and C) and object-based approaches to the classification (Fig. 2B and D). While the principal components were used to train the neural network model, the full spectral reflectance indicates regions of the spectra with the greatest difference between liana-free and severely liana infested trees. Furthermore, standardised reflectance removes the signal of reflectance magnitude making these differences more apparent. The spectral reflectance for severely liana-infested trees was greater across all spectral bands in comparison to liana-free trees (Fig. 2C and D). The regions of the spectra that were most efficient for distinguishing lianas from trees peaked in the visible (546–574 nm) and near-infrared (893–916 nm) for pixel- and object-based approaches, respectively.

Predicted and observed liana canopy cover

A scatterplot of observed and predicted liana infestation revealed a better fit with a pixel-based approach (RMSD = 27.0% ± 0.80; Fig. 3A) compared to an object-based approach (RMSD = 32.6% ± 4.84; Fig. 3B). However, the accuracy of predicted liana infestation when partitioned into three classes [≤30%, 31%–69%, ≥70%] did not differ between pixel- and object-based approaches (McNemar's $\chi^2 = 0.211$, $P = 0.65$, Table 2).

Model outputs and uncertainty

Both pixel- and object-based approaches produced similar patterns of predicted liana infestation across the landscape (Fig. 4A). An increase in liana infestation was generally

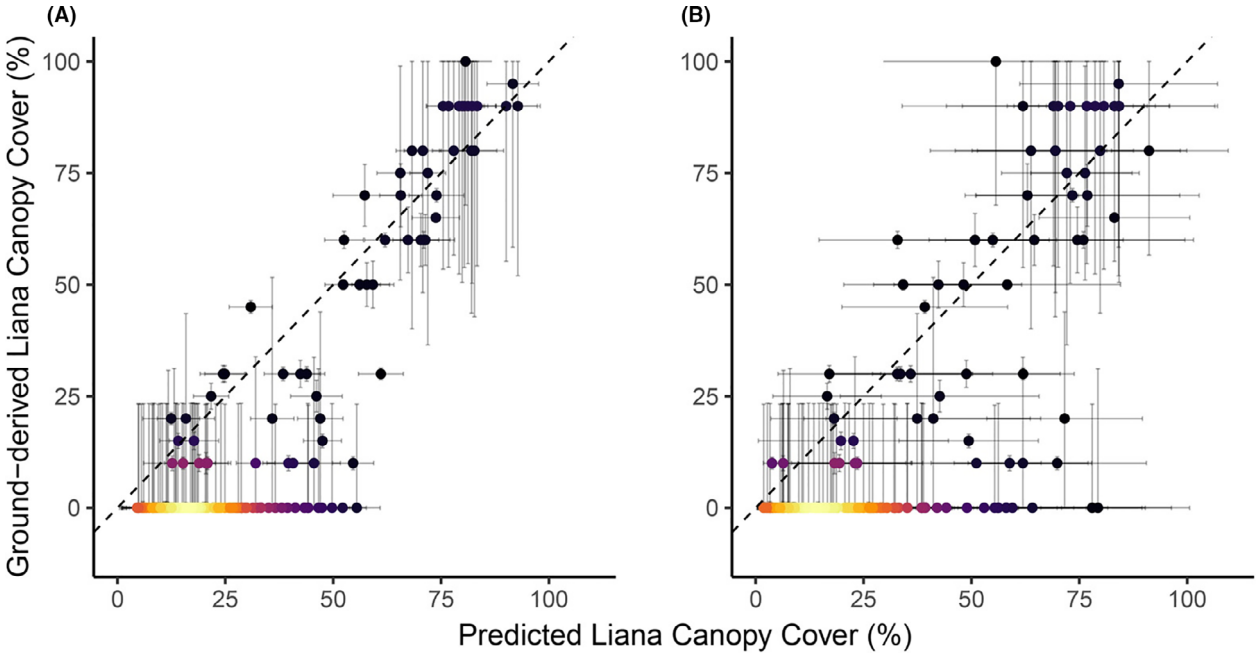

Figure 3. Relationship between predicted and ground reference liana canopy cover for (A) a pixel-based approach and (B) an object-based approach on a continuous scale. Black dashed line represents a 1:1 line. Coloured points correspond to the density of points, ranging from purple to white with an increasing number of overlapping points. Horizontal error bars represent the standard deviation of 100 predicted values generated from multiple iterations of the neural network model. Vertical error bars represent the standard deviation of 100 randomly generated liana canopy cover values using Monte Carlo simulations.

Table 2. Accuracy assessment of pixel- and object-based model outputs.

Model output	Classification	AUC	Accuracy (95% CI)	RMSD
No error applied to validation data				
Output P	Pixel	0.88	0.78 (0.71–0.84)	20.5
Output O	Object	0.84	0.70 (0.63–0.77)	25.1
Error applied to validation data over 100 runs				
Output P	Pixel	0.74 ± 0.03	0.71 ± 0.02	27.0 ± 0.80
Output O	Object	0.68 ± 0.19	0.61 ± 0.18	32.6 ± 4.84

AUC, area under the curve; RMSD, root mean squared deviation.

associated with a decrease in canopy height (Fig. S1). The use of multiple neural network models allowed for a calculation of uncertainty around overall predictions (Fig. 5). We found a pixel-based classification to predict liana infestation with less uncertainty in comparison to an object-based classification (Figs. 3 and 5).

Discussion

Here, we show, for the first time, that despite a lower spectral contrast between liana-free and highly liana infested tree crowns compared to seasonally dry forests (Castro-Esau et al., 2004; Marvin et al., 2016; Sánchez-Azofeifa et al., 2009), airborne remotely sensed imagery and a neural network machine learning classification can be used to assess liana infestation at a landscape-level across an aseasonal forest. Our work therefore extends previous research using similar methodologies to predict liana infestation in seasonally dry forests (Foster et al., 2008; Li et al., 2018; Marvin et al., 2016).

Additionally, we utilised two different approaches in an attempt to overcome some of the methodological issues associated with a difference in scale between remotely sensed data and canopy observations of liana infestation. A pixel-based classification approach revealed a stronger relationship with reference data (RMSD = 27.0% ± 0.80) in comparison with an object-based approach (RMSD = 32.6% ± 4.84; Fig. 3). Furthermore, a pixel-based approach revealed less variation in predictions compared to an object-based approach (Fig. 5).

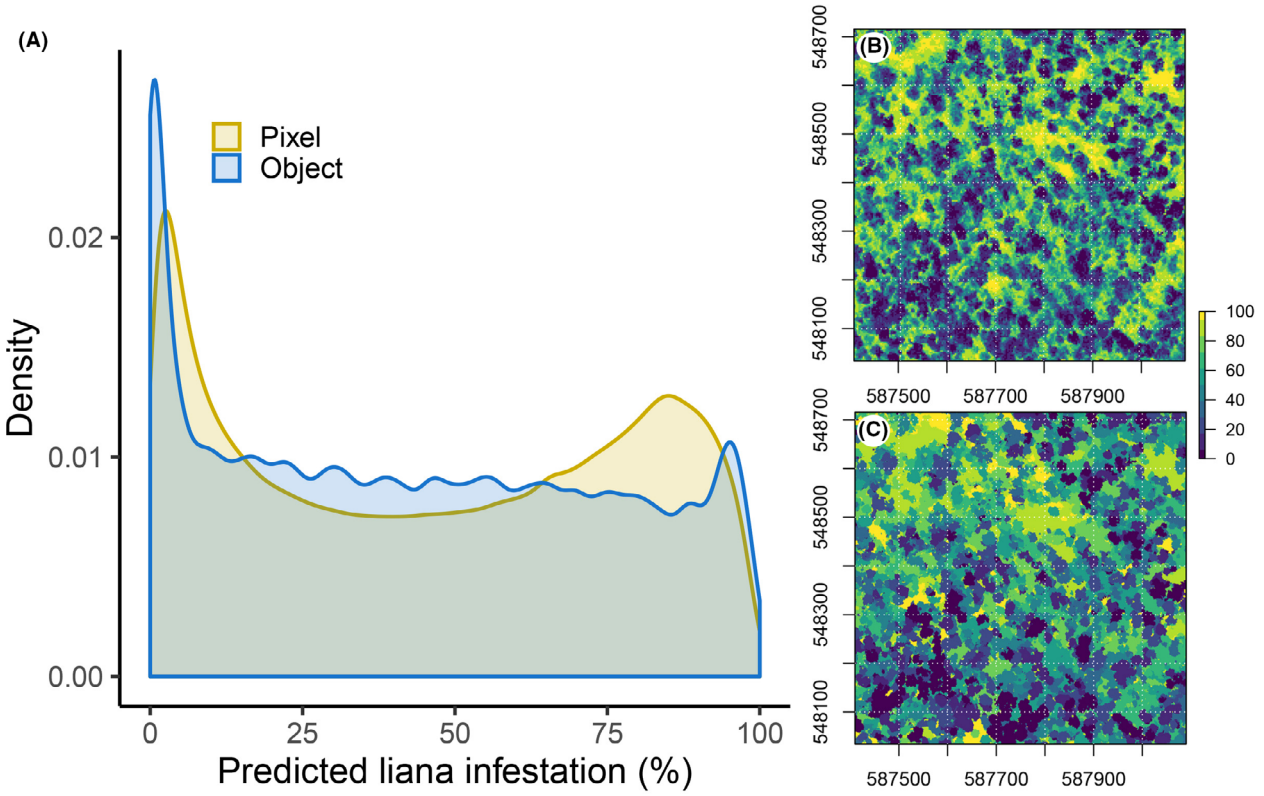

Figure 4. Predicted liana infestation showing (A) the distribution of values for a pixel- (yellow line) and object-based (blue line) classifications, as well as the model predictions for a section of the study area for (B) pixel and (C) object-based classifications, respectively.

While the change in spatial units from pixels to objects reduced within-class spectral variation (Fig. 2), error associated with under-segmentation, that is objects that cover more than one class, may have resulted in large differences in predictions for segmented objects (Liu & Xia, 2010). The overall effects of both over- and under-segmentation present a key limitation for object-based classifications. Therefore, while utilising the entire tree canopy may offer a more attractive approach in theory, the success of this approach, in dense tropical forests, depends greatly on the segmentation process to accurately define objects.

We found a noticeable over-prediction of liana canopy cover for observed estimates below 30% infestation (Fig. 3). This finding is similar to others that have found greater error in the discrimination of tree crowns with liana coverage below 25% - 40% from tree crowns with no liana infestation (Kalacska et al., 2007; Marvin et al., 2016). Where liana infestation is low or absent in a tree canopy, spectral reflectance contaminated by exposed branches, epiphytes or tree trunks may affect the prediction of liana infestation.

Several other factors may have influenced the accuracy of predicted liana infestation in this study. First, we often observed tall, emergent dipterocarps to be liana-free. However, the accuracy of liana infestation estimates may be reduced when assessing tall canopy and emergent trees from the ground due to the greater distance between the observer and tree crown (Waite et al., 2019). As a result, error in liana canopy cover estimates for tall trees may have been introduced in the training data which could affect the accurate prediction of liana infestation. In such cases, or when trees are obscured, unoccupied aerial vehicles have proven to be an effective tool for accurate liana infestation assessment (Waite et al., 2019). Furthermore, tall dipterocarps which typically have large, emergent crowns will likely mask liana infestation in tree canopies directly beneath. Liana infestation of the upper canopy, as assessed by an airborne platform, may therefore underestimate the amount of liana infestation in the forest canopy as a whole.

Second, hyperspectral data were collected in 2014 whereas ground-based estimates of liana canopy cover were collected between 2017 and 2019. Data from Wright et al. (2015) indicated around 2% of all trees that had no liana infestation had become severely (≥75%) liana infested, and vice versa, over a 12-year period. We therefore suggest that liana canopy cover estimates may not

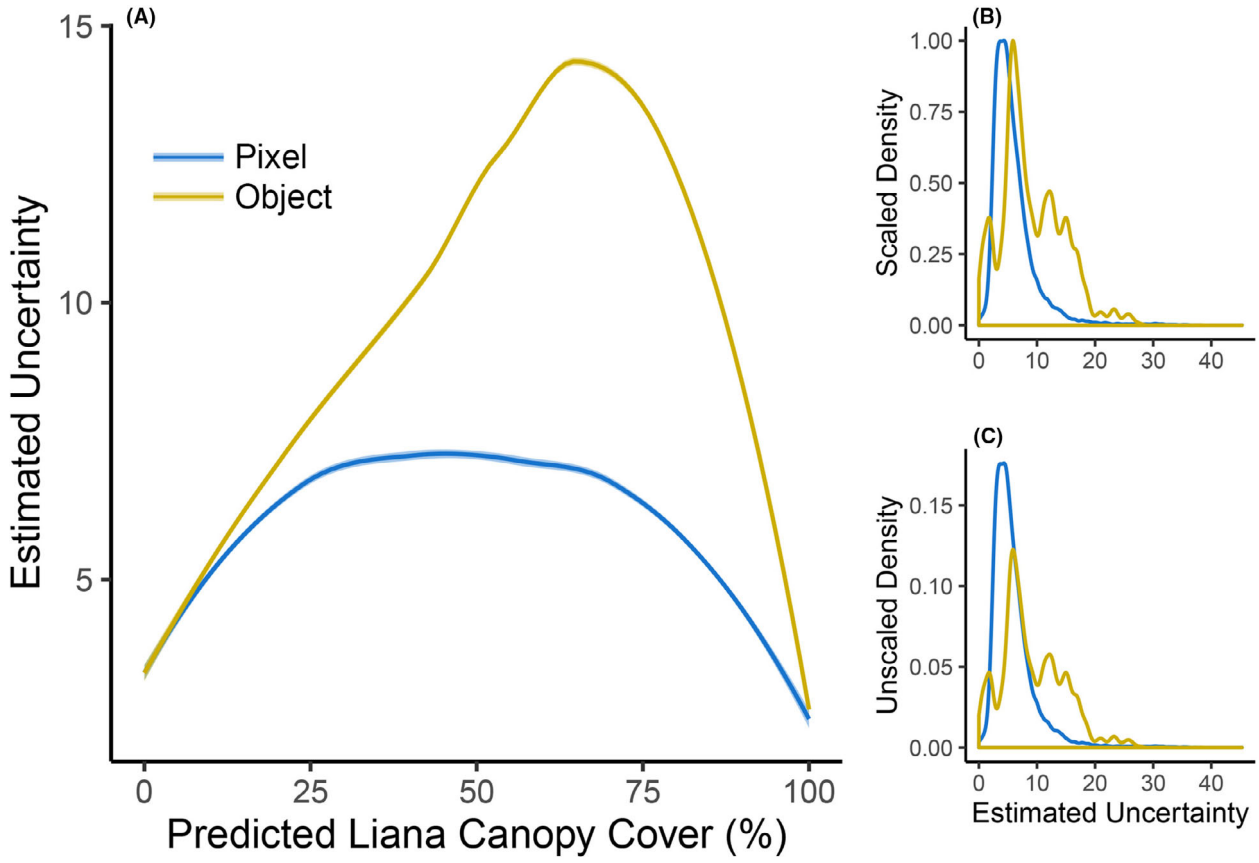

Figure 5. Estimated uncertainty for both model outputs. (A) shows the relationship between estimated uncertainty and predicted liana infestation, (B) and (C) show the scaled and unscaled frequency of uncertainty values across the study area, respectively. Estimated uncertainty was calculated based on the standard deviation of predicted values over 100 neural network models. Fitted lines are produced using a local regression (loess) with 95% confidence interval. Note, the confidence intervals are not visible due to the large sample size.

have varied considerably over a 3.5-year period. Nevertheless, we accounted for error associated with temporal change and field observations of liana canopy cover to quantify uncertainty in predictions of liana infestation. We found that accounting for this error did not substantially alter predicted liana infestation (Figs. S2–S5). While a small degree of error will ultimately be present in the final predicted liana infestation output, the effect on the accuracy of predictions for low liana infestation versus high or severely liana infested trees should be minimal (Fig. 3). This study demonstrates a method that can accurately assess the spatial distribution of liana infestation and should be beneficial for future studies that aim to assess patterns of liana infestation at landscape-scales.

Our method shows that we can identify tree crowns and pixels with liana infestation greater than 30% with a high degree of accuracy (Fig. 3). Accurately identifying trees with more than 50% of their crown covered is essential as previous research has indicated that the impact of lianas on growth, survival and fecundity is greatest for those trees that have more than 50% of their crown covered by liana leaves (Ingwell et al., 2010; Wright et al., 2015). Information on the spatial distribution of high liana infestation may be particularly important for targeted conservation and restoration efforts, especially when geared toward increasing the carbon storage and sequestration potential of tropical forests for climate change mitigation (Addo-Fordjour et al., 2014; Bongers et al., 2002). For example, one of the methods deployed to increase carbon storage and uptake in tropical forests is liana removal (van der Heijden et al., 2015, Marshall et al. 2017). However, blanket liana cutting can be expensive, particularly when it needs to be carried out over large areas or more than once to be effective (Gerwing & Vidal, 2002; Parren & Bongers, 2001; Schnitzer & Bongers, 2005). Being able to accurately locate areas with high liana infestation may therefore help target liana cutting to areas where it is most beneficial and inform efficient forest management and conservation action.

Our findings have demonstrated that remote sensing technologies are capable of accurately detecting liana infestation across an aseasonal tropical forest. As the spectral response of lianas in comparison to trees (Fig. 2) closely resembled results derived from seasonal forests (Marvin et al., 2016), this method may be broadly applicable to other forest locations and types. The approaches used in this study also revealed limitations, suggesting certain approaches may be more suited to one environment over another. For example, the accuracy of segmentation is critical for an object-based approach, which may only be achievable in a primary forest, where there is greater heterogeneity in the canopy in comparison to logged forests (Numata et al., 2006). In secondary forests, where tree and canopy dimensions are typically more homogenous, a pixel-based approach may be more suitable. In addition, the requirement for a liana infestation output may guide the decision to adopt a pixel- or object-based approach. The use of an object-based liana infestation output may be more relatable for forest managers or conservationists that are interested in locating specific trees which are liana-free or heavily liana infested. Similarly, monitoring change in liana infestation over time, or assessing tree mortality as a result of liana infestation, may favour an object-based approach as change is interpreted at the tree-level. However, relating liana infestation to an above ground biomass map or species diversity may benefit from a pixel-based approach, to allow estimates to be generated at scales which can be aligned for meaningful comparisons.

Conclusion

The assessment of liana infestation at the landscape scale is essential to understand the mechanisms that drive spatial patterns of liana coverage, monitor changes over time and quantify the impact on carbon storage and sequestration. By combining airborne hyperspectral and LiDAR data with a neural network classification approach, we have demonstrated the ability to detect and assess liana infestation in an aseasonal tropical environment, where the spectral contrast between lianas and trees is low. Due to potential limitations in the accurate segmentation of tree canopies required for an object-based approach, a pixel-based classification revealed a higher accuracy in predicting liana infestation at a landscape-level. This study advances our ability to assess spatial patterns of liana infestation at the landscape-level, particularly for high (>50%) liana infestation where the impact on carbon storage and sequestration is more pronounced. Being able to detect liana infestation in a tropical forest landscape provides a valuable tool for targeted conservation action and effective forest management focused on liana assessment and control.

Acknowledgements

The authors thank all the research assistants and staff at Danum Valley as well as supporting agencies Sabah Biodiversity Center, Danum Valley Management Committee, Sabah Forestry Department and the Chief Minister's Department Office of Internal Affairs & Research for providing logistical support. The authors also thank Sebastian Böck for providing R code used for segmentation accuracy assessment and Liam Clark for the pre-processing of hyperspectral imagery.

The authors also thank the Natural Environment Research Council [NE/P004806/1 to MEJC, DSB, GMF, GMFvdH; NE/I528477/1 (ARSF MA14/11) to MEJC, DSB, GMF and NE/L002604/1 to CJC, GMF, GMFvdH]. The FCT (Fundação para a Ciência e a Tecnologia) under the project UIDB/04152/2020 – Centro de Investigação em Gestão de Informação (MagIC) to HC. The authors also thank the University of Nottingham for an Anne McLaren Research Fellowship to GMFvdH which funded the collection of the ground data.

Author Contributions

CJC, GMFvdH, DSB and GMF designed the research. CJC collected ground-derived liana canopy cover data. HC performed image segmentation and its respective accuracy assessment. CJC led the writing of the manuscript. All authors contributed critically to the draft manuscripts and gave final approval for publication.

Data Availability Statement

All the data presented here are accessible on Dryad Digital Repository: https://doi.org/.

References

Adam, H., Csaplovics, E. & Elhaja, M. (2016) A comparison of pixel-based and object-based approaches for land use land cover classification in semi-arid areas, Sudan. *IOP Conference Series: Earth and Environmental Science*, **37**, 012061.

Addo-Fordjour, P., Rahmad, Z. & Shahrul, A. (2014) Impacts of forest management on community assemblage and carbon stock of lianas in a tropical lowland forest, Malaysia. *Tropical Conservation Science*, **7**, 244–259.

Blaschke, T. (2010) Object based image analysis for remote sensing. *ISPRS Journal of Photogrammetry and Remote Sensing*, **65**, 2–16.

Bongers, F., Schnitzer, S. & Traore, D. (2002) *The importance of lianas and consequences for forest management in West Africa*, pp. 59–70. Bioterre: revue internationale scientifique de la vie et de la terre. http://www.dow.wau.nl/forestry/pdf-files/bongers-schnitzer2002.pdf.

Castro-Esau, K.L., Sánchez-Azofeifa, G. & Caelli, T. (2004) Discrimination of lianas and trees with leaf-level hyperspectral data. *Remote Sensing of Environment*, **90**, 353–372.

Chang, H. & Yoon, W.S. (2003) Improving the classification of LANDSAT data using standardized principal components analysis. *KSCE Journal of Civil Engineering*, **7**, 469–474.

Chen, Y., Zhou, Y., Ge, Y., An, R.. & Chen, Y.. (2018) Enhancing land cover mapping through integration of pixel-based and object-based classifications from remotely sensed imagery. *Remote Sensing*, **10**, 77.

Costa, H., Foody, G.M. & Boyd, D.S. (2018) Supervised methods of image segmentation accuracy assessment in land cover mapping. *Remote Sensing of Environment*, **205**, 338–351.

Dalling, J.W., Schnitzer, S.A., Baldeck, C., Harms, K.E., John, R., Mangan, S.A. et al. (2012) Resource-based habitat associations in a neotropical liana community. *Journal of Ecology*, **100**, 1174–1182.

Durán, S.M. & Gianoli, E. (2013) Carbon stocks in tropical forests decrease with liana density. *Biology Letters*, **9**, 20130301.

Fick, S.E. & Hijmans, R.J. (2017) WorldClim 2: new 1-km spatial resolution climate surfaces for global land areas. *International Journal of Climatology*, **37**, 4302–4315.

Foody, G.M. (1997) Fully fuzzy supervised classification of land cover from remotely sensed imagery with an artificial neural network. *Neural Computing & Applications*, **5**, 238–247.

Foody, G.M. (2000) Mapping land cover from remotely sensed data with a softened feedforward neural network classification. *Journal of Intelligent and Robotic Systems*, **29**, 433–449.

Foster, J.R., Townsend, P.A. & Zganjar, C.E. (2008) Spatial and temporal patterns of gap dominance by low-canopy lianas detected using EO-1 Hyperion and Landsat Thematic Mapper. *Remote Sensing of Environment*, **112**, 2104–2117.

Gauch, H.G., Hwang, J.T. & Fick, G.W. (2003) Model evaluation by comparison of model-based predictions and measured values. *Agronomy Journal*, **95**, 1442–1446.

Gerwing, J.J. & Vidal, E. (2002) Changes in liana abundance and species diversity eight years after liana cutting and logging in an eastern Amazonian forest. *Conservation Biology*, **16**, 544–548.

Guzman, Q.J., Rivard, B. & Sánchez-Azofeifa, G.A. (2018) Discrimination of liana and tree leaves from a Neotropical Dry Forest using visible-near infrared and longwave infrared reflectance spectra. *Remote Sensing of Environment*, **219**, 135–144.

Hesketh, M. & Sánchez-Azofeifa, G.A. (2012) The effect of seasonal spectral variation on species classification in the Panamanian tropical forest. *Remote Sensing of Environment*, **118**, 73–82.

Ingwell, L.L., Joseph Wright, S., Becklund, K.K., Hubbell, S.P. & Schnitzer, S.A. (2010) The impact of lianas on 10 years of tree growth and mortality on Barro Colorado Island, Panama. *Journal of Ecology*, **98**, 879–887.

Isenburg, M. (2014) *LAStools—efficient LiDAR processing software*. Available at: http://lastools.org [Accessed 10th October 2017].

Jakubowski, M., Li, W., Guo, Q. & Kelly, M. (2013) Delineating individual trees from LiDAR data: a comparison of vector-and raster-based segmentation approaches. *Remote Sensing*, **5**, 4163–4186.

Jing, L., Hu, B., Li, H., Li, J. & Noland, T. (2014) Automated individual tree crown delineation from LIDAR data using morphological techniques. *IOP conference series: earth and environmental science*, pp. 012152. Bristol, UK: IOP Publishing.

Kalacska, M., Bohlman, S., Sanchez-Azofeifa, G.A., Castro-Esau, K. & Caelli, T. (2007) Hyperspectral discrimination of tropical dry forest lianas and trees: comparative data reduction approaches at the leaf and canopy levels. *Remote Sensing of Environment*, **109**, 406–415.

Li, W., Campos-Vargas, C., Marzahn, P. & Sanchez-Azofeifa, A. (2018) On the estimation of tree mortality and liana infestation using a deep self-encoding network. *International Journal of Applied Earth Observation and Geoinformation*, **73**, 1–13.

Li, X. & Shao, G. (2014) Object-based land-cover mapping with high resolution aerial photography at a county scale in midwestern USA. *Remote Sensing*, **6**, 11372–11390.

Liu, D. & Xia, F. (2010) Assessing object-based classification: advantages and limitations. *Remote Sensing Letters*, **1**, 187–194.

Lu, L., Zeng, X., Wu, S. & Zhong, S. (2008) A novel ensemble approach for improving generalization ability of neural networks. *International conference on intelligent data engineering and automated learning*, pp. 164–171. Berlin, Heidelberg: Springer.

Marshall, A. R., M. A. Coates, J. Archer, E. Kivambe, H. Mnendendo, S. Mtoka, et al.2017. Liana cutting for restoring tropical forests: a rare palaeotropical trial. *African Journal of Ecology* **55**, 282–297.

Marvin, D.C., Asner, G.P. & Schnitzer, S.A. (2016) Liana canopy cover mapped throughout a tropical forest with high-fidelity imaging spectroscopy. *Remote Sensing of Environment*, **176**, 98–106.

Meyer, L., Diniz-Filho, J.A.F., Lohmann, L.G., Hortal, J., Barreto, E., Rangel, T. et al. (2019) Canopy height explains species richness in the largest clade of Neotropical lianas. *Global Ecology and Biogeography*, **29**, 26–37. https://doi.org/10.1111/geb.13004.

Numata, S., Yasuda, M., Okuda, T., Kachi, N. & Supardi, M.N. (2006) Canopy gap dynamics of two different forest stands in a Malaysian lowland rain forest. *Journal of Tropical Forest Science*, 109–116.

Nunes, M., Ewers, R., Turner, E. & Coomes, D. (2017) Mapping aboveground carbon in oil palm plantations using

LiDAR: a comparison of tree-centric versus area-based approaches. *Remote Sensing*, **9**, 816.

O'Brien, M.J., Philipson, C.D., Reynolds, G., Dzulkifli, D., Snaddon, J.L., Ong, R. et al. (2019) Positive effects of liana cutting on seedlings are reduced during El Niño-induced drought. *Journal of Applied Ecology*, **56**, 891–901.

Olofsson, P., Foody, G.M., Herold, M., Stehman, S.V., Woodcock, C.E. & Wulder, M.A. (2014) Good practices for estimating area and assessing accuracy of land change. *Remote Sensing of Environment*, **148**, 42–57.

Olson, M., Wyner, A. & Berk, R. (2018) Modern neural networks generalize on small data sets. *Advances in Neural Information Processing Systems*, 3619–3628.

Pan, Y., Birdsey, R.A., Fang, J., Houghton, R., Kauppi, P.E., Kurz, W.A. et al. (2011) A large and persistent carbon sink in the world's forests. *Science*, **333**, 988–993.

Parren, M. & Bongers, F. (2001) Does climber cutting reduce felling damage in southern Cameroon? *Forest Ecology and Management*, **141**, 175–188.

Phillips, O.L., Martínez, R.V., Arroyo, L., Baker, T.R., Killeen, T., Lewis, S.L. et al. (2002) Increasing dominance of large lianas in Amazonian forests. *Nature*, **418**, 770–774.

Piñeiro, G., Perelman, S., Guerschman, J.P. & Paruelo, J.M. (2008) How to evaluate models: observed vs. predicted or predicted vs. observed? *Ecological modelling*, **216**, 316–322.

Plaza, J., Hendrix, E.M., García, I., Martín, G. & Plaza, A. (2012) On endmember identification in hyperspectral images without pure pixels: a comparison of algorithms. *Journal of Mathematical Imaging and Vision*, **42**, 163–175.

Putz, F.E. (1984) The natural history of lianas on Barro Colorado Island, Panama. *Ecology*, **65**, 1713–1724.

QGIS Development Team. (2018) QGIS geographic information system. *Open Source Geospatial Foundation Project*.

R Core Team. (2019) *R: a language and environment for statistical computing*. Vienna, Austria: R Foundation for Statistical Computing. Available at: https://www.R-project.org/.

Reynolds, G., Payne, J., Sinun, W., Mosigil, G. & Walsh, R.P. (2011) Changes in forest land use and management in Sabah, Malaysian Borneo, 1990–2010, with a focus on the Danum Valley region. *Philosophical Transactions of the Royal Society B: Biological Sciences*, **366**, 3168–3176.

Sánchez-Azofeifa, G. & Castro-Esau, K. (2006) Canopy observations on the hyperspectral properties of a community of tropical dry forest lianas and their host trees. *International Journal of Remote Sensing*, **27**, 2101–2109.

Sánchez-Azofeifa, G.A., Castro-Esau, K., Wright, S.J., Gamon, J., Kalacska, M., Rivard, B. et al. (2009) Differences in leaf traits, leaf internal structure, and spectral reflectance between two communities of lianas and trees: implications for remote sensing in tropical environments. *Remote Sensing of Environment*, **113**, 2076–2088.

Schnitzer, S.A. (2005) A mechanistic explanation for global patterns of liana abundance and distribution. *The American Naturalist*, **166**, 262–276.

Schnitzer, S.A. & Bongers, F. (2005) Lianas and gap-phase regeneration: implications for forest dynamics and species diversity. Pp. 59–72 *in* F Bongers, M.P.E Parren and D Traore, eds. *Forest climbing plants of West Africa: Diversity, ecology, and management*. Wallingford: CABI Publishing.

Schnitzer, S.A. & Bongers, F. (2011) Increasing liana abundance and biomass in tropical forests: emerging patterns and putative mechanisms. *Ecology Letters*, **14**, 397–406.

Schnitzer, S.A. & Carson, W.P. (2010) Lianas suppress tree regeneration and diversity in treefall gaps. *Ecology Letters*, **13**, 849–857.

Schnitzer, S.A., Mangan, S.A., Dalling, J.W., Baldeck, C.A., Hubbell, S.P., Ledo, A. et al. (2012) Liana abundance, diversity, and distribution on Barro Colorado Island, Panama. *PLoS One*, **7**, e52114.

Schnitzer, S.A. & van der Heijden, G.M. (2019) Lianas have a seasonal growth advantage over co-occurring trees. *Ecology*, **100**, e02655.

Shao, Y. & Lan, J. (2019) A spectral unmixing method by maximum margin criterion and derivative weights to address spectral variability in hyperspectral imagery. *Remote Sensing*, **11**, 1045.

Stehman, S.V. & Foody, G.M. (2019) Key issues in rigorous accuracy assessment of land cover products. *Remote Sensing of Environment*, **231**, 111199.

Stevens, G.C. (1987) Lianas as structural parasites: the Bursera simaruba example. *Ecology*, **68**, 77–81.

Taylor. (2001) Strategies for overcoming problems when mosaicking airborne scanner images. *Earth Observation Magazine*, **10**, 26–31.

Tymen, B., Réjou-Méchain, M., Dalling, J.W., Fauset, S., Feldpausch, T.R., Norden, N. et al. (2016) Evidence for arrested succession in a liana-infested Amazonian forest. *Journal of Ecology*, **104**, 149–159.

van der Heijden, G.M. & Phillips, O. (2009) Liana infestation impacts tree growth in a lowland tropical moist forest. *Biogeosciences*, **6**, 2217–2226.

van der Heijden, G.M., Powers, J.S. & Schnitzer, S.A. (2015) Lianas reduce carbon accumulation and storage in tropical forests. *Proceedings of the National Academy of Sciences*, **112**, 13267–13271.

Waite, C.E., van der Heijden, G.M., Field, R. & Boyd, D.S. (2019) A view from above: unmanned aerial vehicles (UAV s) provide a new tool for assessing liana infestation in tropical forest canopies. *Journal of Applied Ecology*, **56**, 902–912. https://doi.org/10.1111/1365-2664.13318.

Wright, S.J., Sun, I., Pickering, M., Fletcher, C.D. & Chen, Y.-Y. (2015) Long-term changes in liana loads and tree dynamics in a Malaysian forest. *Ecology*, **96**, 2748–2757.

Yang, J., He, Y., Caspersen, J. & Jones, T. (2015) A discrepancy measure for segmentation evaluation from the perspective of object recognition. *ISPRS Journal of Photogrammetry and Remote Sensing*, **101**, 186–192.

Yu, C.-C. & Liu, B.-D. (2002) A backpropagation algorithm with adaptive learning rate and momentum coefficient. Pp. 1218–1223 *in Proceedings of the 2002 International Joint Conference on Neural Networks. IJCNN'02 (Cat. No. 02CH37290)*, vol. **2**. Honolulu, HI, USA: IEEE. https://doi.org/10.1109/IJCNN.2002.1007668.

Yu, Q., Gong, P., Clinton, N., Biging, G., Kelly, M. & Schirokauer, D. (2006) Object-based detailed vegetation classification with airborne high spatial resolution remote sensing imagery. *Photogrammetric Engineering & Remote Sensing*, **72**, 799–811.

Supporting Information

Additional supporting information may be found online in the Supporting Information section at the end of the article.

Figure S1. Relationship between liana canopy cover (%) and canopy height (m) for (A) pixel- and (B) object-based data. Red dashed line corresponds to a fitted linear regression.

Figure S2. Relationship between predicted and ground reference liana canopy cover for the first 10 of the 100 iterations of the modelling process using a pixel-based approach.

Figure S3. Relationship between predicted and ground reference liana canopy cover for the first 10 of the 100 iterations of the modelling process using an object-based approach.

Figure S4. Neural network error (green) and accuracy of predicted liana infestation (orange) in response to an incremental increase in error from 0% to 50% applied to the input data over 100 iterations.

Figure S5. The difference in estimates of liana canopy cover by two observers.

Figure S6. Average monthly rainfall (mm) at the Danum Valley Field Centre (DVFC) from 1986-2016. Data from Chappell (2016).

Data S1. Supplementary materials.

